Measurement of matter-antimatter asymmetries with the LHCb experiment

Lukas Bertsch
lukas.bertsch@tu-dortmund.de

Tabea Hacheney
tabea.hacheney@tu-dortmund.de

Tom Troska
tom.troska@tu-dortmund.de

Start of course: 24th of May 2024

TU Dortmund University – Faculty of Physics

Contents

1 Motivation

In our universe, we observe a surplus of particles over antiparticles that is called *baryon asymmetry*. A key aspect of this matter-antimatter problem is the violation of the *CP* symmetry that occures in the weak interaction. In this experiment, the decays of B mesons measured by the LHCb experiment are analyzed to calculate the *CP* asymmetry.

2 Theory

In 1964, *CP* violation was observed for the first time by Cronin and Fitch [5] in the decay of neutral Kaons. At this time, the Standard Model of particle physics did not provide methods to describe *CP* violation. This chapter focuses on establishing a connection between the baryon asymmetry and the violation of the *CP* symmetry. Moreover, the theory behind *CP* violation is explained.

2.1 Sakharov conditions

For a higher production rate of matter over antimatter, three conditions must be fullfilled. These conditions are referred to as the *Sakharov conditions*, named after the physicist Andrei Sakharov who proposed these criteria in 1966 [9]. First, a violation of the baryon number B is needed. This is in disagreement with the Standard Model as we know it today but extensions of it could allow for baryon number violation.
Second, both the charge symmetry C and the combination of the charge and parity symmetries *CP* need to be violated. The *CP* violation is the topic of this lab course and is explained in detail in the following sections.
The third conditon states that the violation of the baryon number (first conditon) needs to occur out of thermal equilibrium. If this was not the true, any baryon number asymmetry would lead to a corresponding reverse process and thus no overall asymmetry could be observed. Consequently, the universe is not in a state of thermal equilibrium.

2.2 *CP* violation in the weak interaction

Before 1970, the weak interaction theory was based on Nicola Cabibbo's notation of the unitary symmetry [4] leading to quark mixing via the Cabibbo angle. This notation described how the weak interaction causes transitions between different quark flavors via

$$u \leftrightarrow d \cdot \cos(\theta_{\mathrm{C}}) \quad \text{and} \quad u \leftrightarrow s \cdot \sin(\theta_{\mathrm{C}}).$$

At this time, only three quarks (u,d,s) were know to be part of the Standard Model. This theory faced issues with renormalizability, failing to adequately describe certain decays or particle interactions. In 1970, Glashow, Iliopoulos, and Maiani proposed a new weak interaction theory [6], introducing a fourth quark (charm) and one vector boson (Z_0). This model helped address these problems and allowed for the integration of the previously predicted boson and the unification with the electroweak interaction. A few years later, in 1973, Kobayashi and Maskawa further refined the theory of the weak

interaction by postullating a third generation of quarks [7]. By introducing the quarks now known as *top* and *bottom* quarks, they also extended the theory to a total of three mixing angles θ_i and a *CP* violating phase δ. In summary, the quark mixing matrix is written as

$$\begin{pmatrix} V_{\mathrm{ud}} & V_{\mathrm{us}} & V_{\mathrm{ub}} \\ V_{\mathrm{cd}} & V_{\mathrm{cs}} & V_{\mathrm{cb}} \\ V_{\mathrm{td}} & V_{\mathrm{ts}} & V_{\mathrm{tb}} \end{pmatrix}.$$

This unitary matrix is referred to as the *Cabibbo-Kobayashi-Maskawa* matrix or the *CKM* matrix and can be parameterized in different manners, for example

$$\begin{pmatrix} c_1 & -s_1 c_3 & -s_1 s_3 \\ s_1 c_2 & c_2 c_2 c_3 - s_2 s_3 \mathrm{e}^{\mathrm{i}\delta} & c_1 c_2 s_3 + s_2 c_3 \mathrm{e}^{\mathrm{i}\delta} \\ s_1 s_2 & c_1 s_2 c_3 + c_2 s_3 \mathrm{e}^{\mathrm{i}\delta} & c_1 s_2 s_3 - c_2 c_3 \mathrm{e}^{\mathrm{i}\delta} \end{pmatrix}.$$

Here, s_i and c_i are abbreviations for sines and cosines of the mixing angles θ_i, e.g. $s_1 = \sin\theta_1$. Another representation of the *CKM* matrix is a form with Euler angles, where θ_{12} denotes the Cabibbo angle θ_{C}. The result is

$$\begin{pmatrix} c_{12}c_{13} & s_{12}c_{13} & s_{13}\mathrm{e}^{-\mathrm{i}\delta_{13}} \\ -s_{12}c_{23} - c_{12}s_{23}s_{13}\mathrm{e}^{\mathrm{i}\delta_{13}} & c_{12}c_{23} - s_{12}s_{23}s_{13}\mathrm{e}^{\mathrm{i}\delta_{13}} & s_{23}c_{13} \\ s_{12}s_{23} - c_{12}c_{23}s_{13}\mathrm{e}^{\mathrm{i}\delta_{13}} & -c_{12}s_{23} - s_{12}c_{23}s_{13}\mathrm{e}^{\mathrm{i}\delta_{13}} & c_{23}c_{13} \end{pmatrix}.$$

In another representation of the matrix, the parameters are chosen such that the unity matrix is obtained in the absence of quark mixing. The four degrees of freedom are expressed as

$$\lambda = s_{12} \qquad\qquad A = \frac{s_{23}}{s_{12}^2}$$

$$\rho = \mathfrak{R}\left(\frac{s_{13}\mathrm{e}^{-\mathrm{i}\delta}}{s_{12}s_{23}}\right) \qquad\qquad \eta = -\mathfrak{I}\left(\frac{s_{13}\mathrm{e}^{-\mathrm{i}\delta}}{s_{12}s_{23}}\right).$$

Inserting these parameters into the *CKM* matrix leads to an approximation to the order λ^3. It follows that

$$\begin{pmatrix} 1 - \frac{1}{2}\lambda^2 & \lambda & A\lambda^3(\rho - \mathrm{i}\eta) \\ -\lambda & 1 - \frac{1}{2}\lambda^2 & A\lambda^2 \\ A\lambda^3(1 - \rho - \mathrm{i}\eta) & -A\lambda^2 & 1 \end{pmatrix}.$$

In this form, the violation of the *CP* symmetry is found in the parameter ρ and η.

2.3 *B* meson decay

The B system is of particular interest for the research of *CP* violation because of the oscillation of the neutral mesons. Here, B_d^0 mesons oscillate into their antiparticle $\bar{B}_d^0$
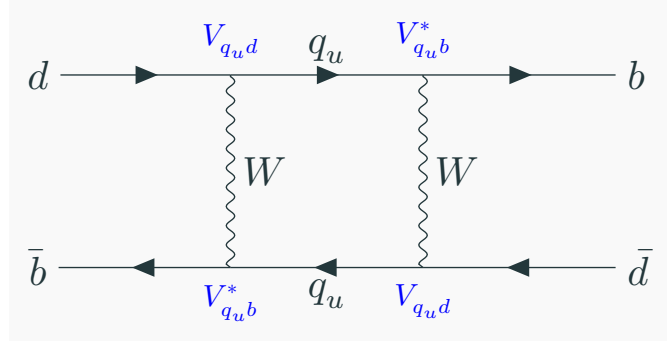
Figure 1: Transition of a B_d^0 meson into a $\bar{B}_d^0$ meson.

and vice versa. The leading order Feynman diagram for this oscillation is depicted in Figure 1.

In the context of this analysis, the *CP* asymmetry is calculated for the decay of B^+ and B^- mesons. In the absence of *CP* violation, the production rates of these two mesons are expected to be identical. Hence, a value for the *CP* violation can be determined by

$$A_{\mathrm{CP}} = \frac{N^+ - N^-}{N^- + N^+}. \tag{1}$$

The number of observed $B^+ \to h^+h^+h^-$ is denoted as N^+, while the matching number of $B^- \to h^+h^-h^-$ is N^-.

3 The LHCb detector

Alongside ALICE, ATLAS and CMS, LHCb is one of the four main experiments located at the Large Hadron Collider (LHC) at CERN. At the LHC, opposing proton beams are brought to collision at the four main interaction points with a bunch collision rate of 40 MHz. The resulting particle cascades can then be measured and analysed using the different experiments. LHCb is designed to measure decays including *b* and *c* quarks which play an important role in the field of *CP* violation.

The detector is a single-arm forward spectrometer with an acceptance of $2 \leq \eta \leq 5$ in the pseudorapidity range. A schematic view of the apparatus as used in the data taking period relevant for this analysis can be seen in Figure 2. The interaction point of the proton-proton collisions is located at the very left of the graphic, at the Vertex Locator (VELO). The VELO's primary purpose is to measure the primary and secondary vertices of decays. It therefore needs to provide a high spatial resolution. This information can then be used to reconstruct the lifetime and impact paramter (IP) of the decays. *B*-mesons, for example, typically decay after a few mm to cm and can therefore be measured in the VELO. The tracking stations TT (Tracker Turicensis) and T1-T3 are used to reconstruct tracks of (charged) particles deflected by the dipole magnet, which has an integrated field strength of 4 T m. The information from the tracking stations can be used to calculate momentum and charge of a particle. The Ring Imaging Cherenkov
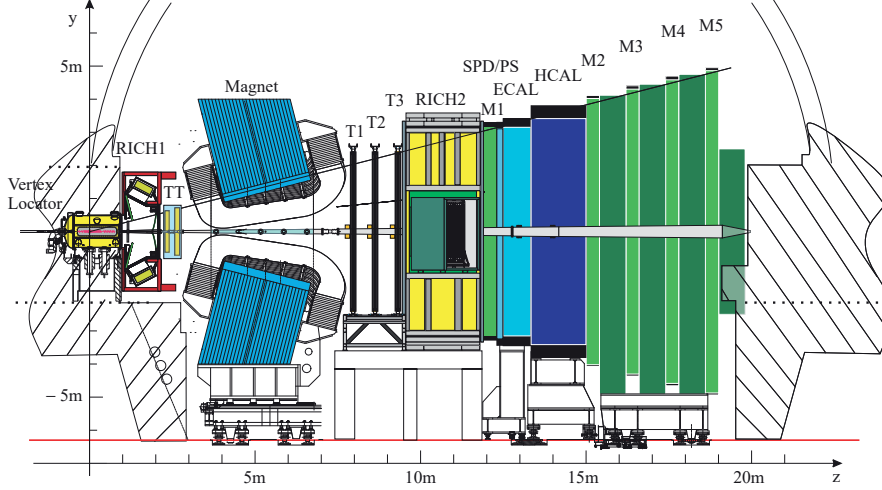
Figure 2: The setup of the Large Hadron Collider beauty experiment as used in Run 1 [2]. The collision point of the protons is on the left. The Vertex Locator (VELO), the tracking stations (TT, T1-T3), the Ring Imaging Cherenkov detectors (RICH1-2), as well as the calorimeters (SPD/PS, ECAL, HCAL) and the muon chambers (M1-M5) can be seen.

detectors RICH 1 and 2 lie upstream and downstream of the tracking stations, respectively. Here, the velocity of traversing particles is calculated from diameter measurements of light cones caused by the Cherenkov effect. Together with the momentum information, this contributes to the particle identification (PID) and can be used to determine kaons from pions. Further downstream, the calorimeter system consisting of the Scintillating Pad Detector (SPD), the Preshower detector (PS) and the electromagnetic- (ECAL) and hadronic (HCAL) calorimeters is located. The calorimeters are utilised to measure the particles energy deposition and also contribute to PID. At the very end of the detector, the muon chambers (M1-M5) measure muons which do not interact much with the aforementioned detector parts.

Events measured by the detector are triggered and preprocessed by a three-level trigger system. The reconstructed decays of interest are then saved to storage for further offline analysis.

4 Analysis strategy

The data used for this analysis was taken in 2011 at a center of mass energy of $7\,\text{TeV}$. It includes 3.4(5.1) million events of $B^{\pm} \to h^{\pm}h^{+}h^{-}$ decays ($h^{\pm}$: hadron; kaon $K^{\pm}/$ pion $\pi^{\pm}$) with dipole magnet polarity up (down), corresponding to an integrated luminosity of $434\,\text{pb}^{-1}$ ($584\,\text{pb}^{-1}$) [8]. Here, only the decay into three kaons ($h^{\pm} = K^{\pm}$) is considered. A dataset of simulated $B^{\pm} \to K^{\pm}K^{+}K^{-}$ decays is also available.

At first, the data is read from the provided `.root` files using the python extension *pyROOT* of the software package *ROOT* [3]. Histograms of the distributions of the

variables listed in the file are to be created for the simulated and measured data. The provided parameters for both simulation and real data are listed in the appendix. The simulated data does not include decays via resonances. Next, the energy of the kaons in the simulated data is calculated using the known kaon mass and its momentum. From this, the invariant mass of the B-mesons can be calculated and histogrammed. The same is done for the measured data after decays with only kaons in the final state are selected using PID information from the variables listed in the dataframe. A high efficiency should be maintained. The differences between the mass distributions of the measured- and simulated data are to be described. Following that, the global CP asymmetry, its uncertainty and significance are calculated. In the next step, Dalitz plots are created for the simulated and experimental data. Using the Dalitz diagrams, charm resonances that are present in the measured data can be identified and removed. Finally, the local CP violation in different areas of the Dalitz plot is to plotted. The areas with the most significant evidence of CP violation should be identified and the significance of CP violation in this areas should be calculated.

5 Analysis

5.1 Kinematics of the simulated data

To get to know the underlying process, the data simulated by Monte Carlo is analysed for its kinematic properties. The vector components of the momentum of one of the hadrons are shown in Figure 3. The momenta in the x- and y- direction follow a gaussian distribution. These two axes are perpendicular to the beam. However, the z-component shows negative exponential behaviour.
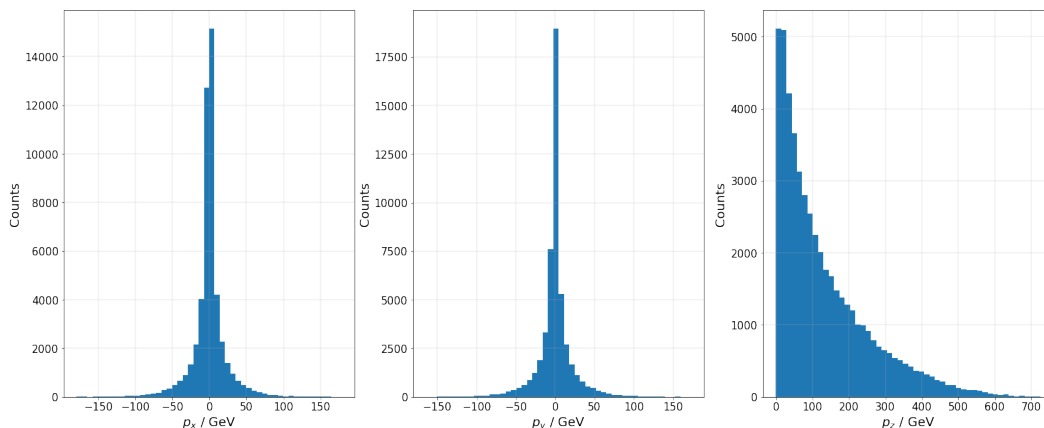

Figure 3: Histograms of the distributions of the momentum vector components for the first hadron of the simulated data.

With these quantities, the magnitude of the momentum can be calculated via

$$p = \sqrt{p_x^2 + p_y^2 + p_z^2}. \tag{2}$$

7

This is done for every kaon candidate and every event. The resulting distribution of the magnitude of the momentum is shown in Figure 4.
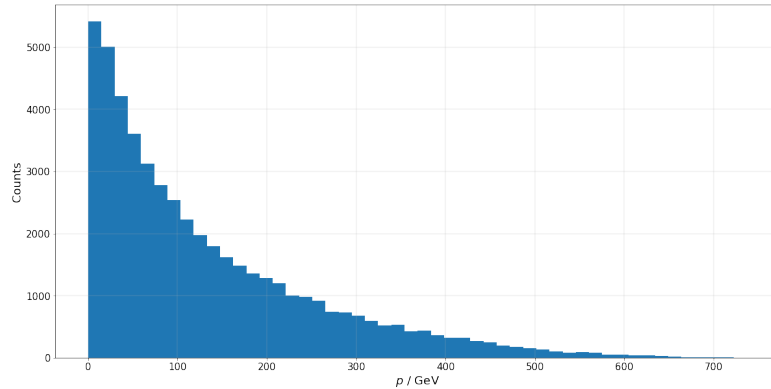

Figure 4: Histogram of the magnitude of the momentum for the first hadron of the simulated data.

By using the realtion of energy, mass and momentum given by

$$E^2 = p^2 + m^2, \tag{3}$$

the energy of the hadrons can be calculated. The kaon mass is well known and documented by the Particle Data Group [10]. It is given by $m_{K^\pm} = (493.677 \pm 0.015)\,\text{MeV}$. The resulting energy distribution of the first hadron is depicted in Figure 5.
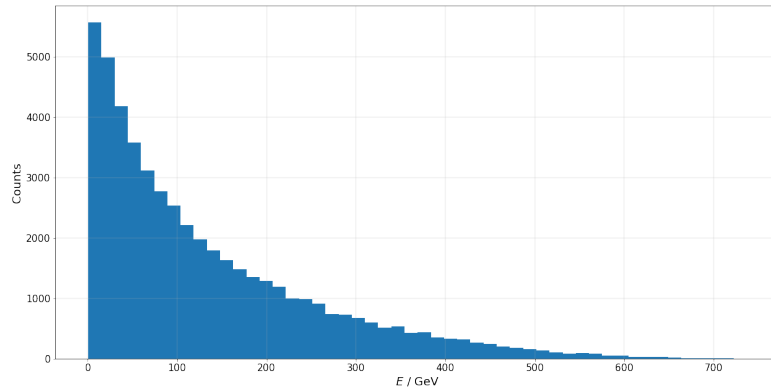

Figure 5: Histogram of the energy of the first hadron of the simulated data.

The energy is also calculated for the other kaon candidates. Since energy and momentum are conserved quantities, the energy and momentum of the $B^\pm$ meson can be calculated using the energy and momentum of the three kaon candidates. The single momentum components of all final state particles are added together and the magnitude of the momentum of the $B^\pm$ meson can be calculated via Equation 2. The energy is calculated by summing the energy of all final state particles. With the energy and the magnitude of

the momentum, the resulting mass of the $B^{\pm}$ meson can be calculated via Equation 3. The resulting distribution can be seen in Figure 6. The distribution has a sharp peak
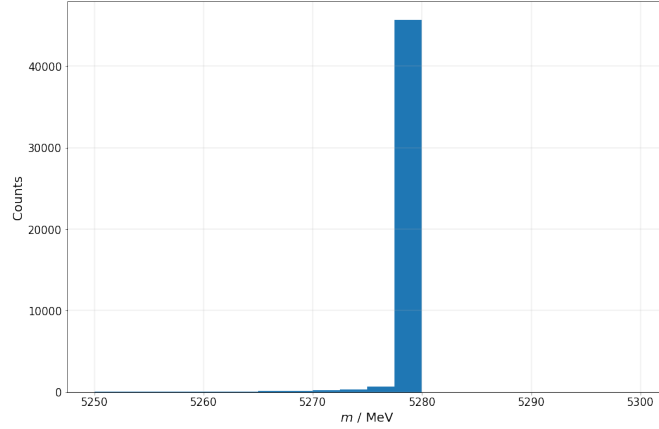

Figure 6: Histogram of the mass of the $B^{\pm}$ meson of the simulated data.

at the mass of the $B^{\pm}$ meson ($m_{B^{\pm}} = (5279.41 \pm 0.07)\,\text{MeV}$ [10]). This is because the data is simulated data using information about the mass of the $B^{\pm}$ meson during the simulation process. The distribution for real data would be a lot broader and will also contain combinatorial background.

5.2 Preselection

To reduce combinatorial background and misidentified decays as well as selecting only the decay into kaons, tighter cuts on the given parameters are needed. By using the distributions of the given parameters (Figure 7), that describe the likeliness of the hadron being a specific particle, one can decide for appropriate cuts. This is done for all three final state hadrons. When choosing the cut, it is important not to cut too tightly. Doing so would reduce the number of signal events and worsen the statistics. Also, to ensure that the hadrons are not muons, the variable `isMuon` is used for the preselection. The chosen cuts are listed in Table 1.

Preselection			
Variable	Hadron 1	Hadron 2	Hadron 3
`isMuon` (boolean)	is not	is not	is not
`ProbK`	> 0.6	> 0.55	> 0.85
`ProbPi`	< 0.3	< 0.3	< 0.3

Table 1: The chosen cuts for the preselection of the recorded data. The values are chosen according to the distributions shown in Figure 7.

The magnitude of the momentum, the energy as well as the mass of the $B^{\pm}$ meson is calculated for the real data, just like it has been done in subsection 5.1 for the simulated
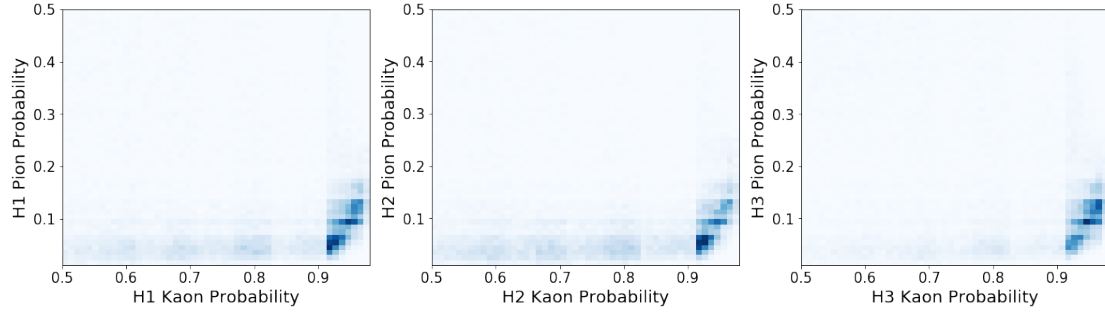
9

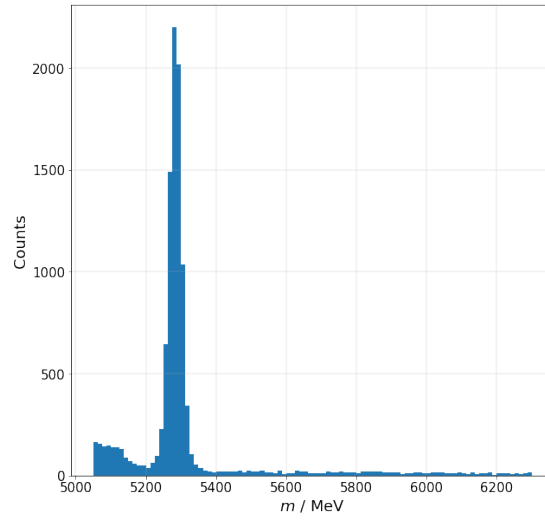**Figure 7:** A 2-dimensional histogram for the Kaon and Pion probability of the three hadrons.

Figure 8: Histogram of the mass of the $B^{\pm}$ meson of the recorded data.

data. The resulting distribution of the $B^{\pm}$ meson mass can be seen in Figure 8.

The gaussian distribution of the mass of the $B^{\pm}$ meson is much broader and also contains uniform background as well as a more dominant background on the lower end of the invariant mass. To reject the background further, a cut on the $B^{\pm}$ meson mass is applied as $m_B > 5200\,\text{MeV}$ and $m_B < 5400\,\text{MeV}$. Multiple cuts are tested. The chosen cuts seem to be the best choice for rejected most background, while maintaining much signal.

5.3 Global matter anti-matter differences

To study possible *CP* violation, the dataset has to be split for events with $B^+ \to K^+ K^+ K^-$ and $B^- \to K^- K^+ K^-$. The $B^{\pm}$ meson charge is established by looking at the charge of the kaon candidates. Those events, which have two negatively charged kaons came from a B^- meson and those with two positively charged kaons from a B^+ meson. The asymmetry is calculated by summing the number of events in each dataset and using Equation 1.

The resulting global asymmetry for the selected events is $A_{CP} = 0.0436$. In particle physics, a value is only considered an observation, if it is at least five standard deviations. If it exceeds three sigma, it is considered evidence. The uncertainty of the asymmetry can be calculated via

$$\sigma_A = \sqrt{\frac{1 - A_{CP}^2}{N^+ + N^-}}. \tag{4}$$

The significance is the asymmetry devided by the resulting uncertainty. The uncertainty for the selected events is $\sigma_A = 0.0109$ and the significance is $S = 4.0041$. The calculated asymmetry can therefore be regarded as evidence.

However, the statistical uncertainty is not the only uncertainty that should be regarded when analysing this decay. The production asymmetry can be approximated with 1% and is substracted from the raw asymmetry. By using Equation 4, the uncertainty for the production asymmetry is $\sigma_P = 0.0109$. Using gaussian error propagation, the improved asymmetry, the final uncertainty, and the significance are

$$A_{CP,\text{global}} = 0.0336,$$
$$\sigma_{A_{CP,\text{global}}} = 0.0154 \text{ and}$$
$$S_{A_{CP,\text{global}}} = 2.181.$$

The result is therefore no longer regarded as evidence.

5.4 Dalitz plots and resonances

The decay $B^{\pm} \to K^{\pm} K^+ K^-$ does not only occur in the direct way. It can also take place via neutral resonances R^0. These resonances are neutral mesons, which then decay into a pair of positively and negatively charged kaons. There are two possible combinations for this, since two kaons always have the same charge. To visualise and make out resonances, a Dalitz plot can be drawn. For the Dalitz plot, the masses for these two resonance

combinations are calculated just like as for the $B^{\pm}$ meson. The squared masses of the two resonance combinations are then plotted against each other in a two dimensional diagram. On this plot, resonances are visible by band structures. Depending on the likeliness of the resonance, these bands can be less or more clear to make out.

For the simulated data, the Dalitz plot is shown in Figure 9a. The simulated data does not include resonances and is therefore uniformly distributed. As for the recorded data, the Dalitz plot is shown in Figure 9b. It is important to first look up, which kaon candidates are oppositely charged. In this case, the second and third kaon candidate have the same charge. Therefore, only the combinations R_{12}^0 and R_{13}^0 are neutral. The combination of the second and third particle would mean, that there was a double positively or negatively charged resonance, which is not possible in the Standard Model.
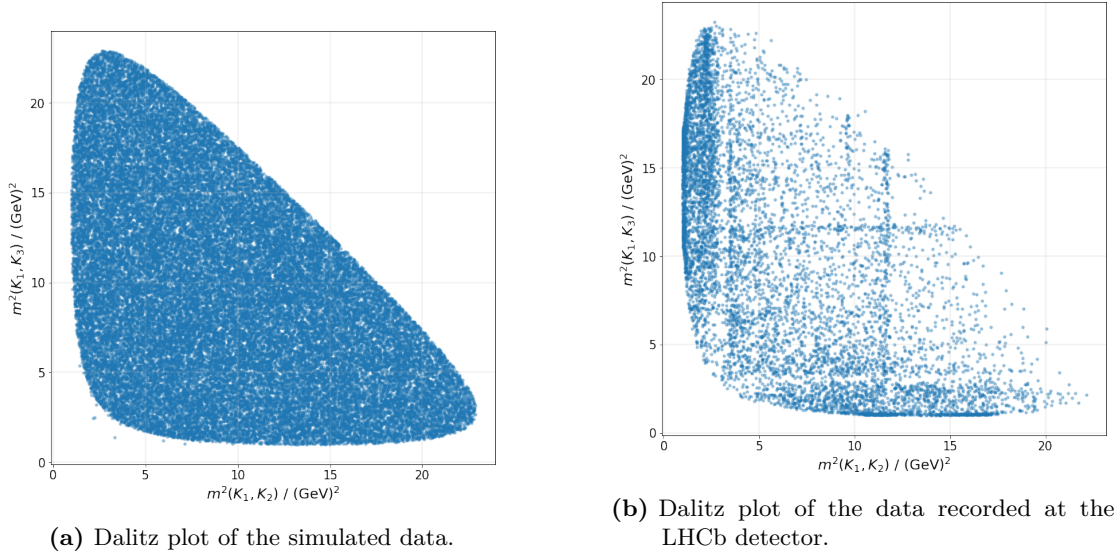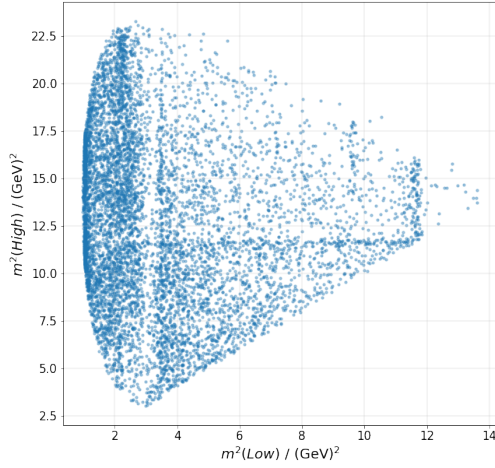

(a) Dalitz plot of the simulated data.

(b) Dalitz plot of the data recorded at the LHCb detector.

Figure 9: Scatter plots of the Dalitz plots for the simulated data and the recorded data.

To make the resonances more visible, it can be helpful to order the resonances by mass. This creates a variable "Low", which always includes the resonance with the lower mass and a variable "High" which includes the resonance with the higher mass. The resulting scatter plot is shown in Figure 10a. Also, a binned histogram of the data helps to show higher local densities. This is shown in Figure 10b. Especially Figure 10a shows two main resonances. One being at approximately $3.5\,\mathrm{GeV}^2$ and one at approximately $11.5\,\mathrm{GeV}^2$. Taking the root of these values gives the mass of the resonances as $R_1^0 \approx 1870\,\mathrm{MeV}$ and $R_2^0 \approx 3390\,\mathrm{MeV}$. As these values got extracted from the plot by eye, the uncertainties are high. By using the PDG [10], one can identify the first resonance R_1^0 as the D^0 meson ($m_{D^0} = (1864.84 \pm 0.05)\,\mathrm{MeV}$[10]) and the second resonance R_2^0 as the χ_{c0} meson ($m_{\chi_{c0}} = (3414.71 \pm 0.30)\,\mathrm{MeV}$[10]).

(a) Dalitz plot of the recorded data.
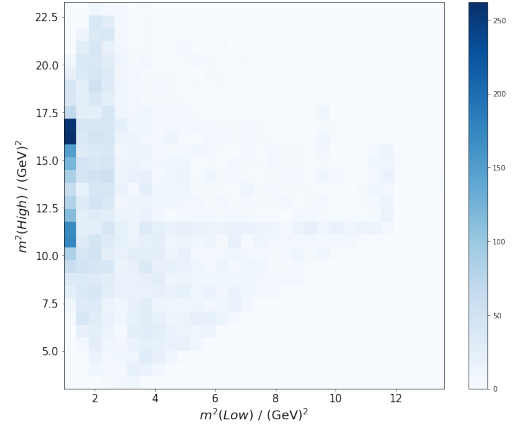
(b) Binned Dalitz plot to visualise local densities.

Figure 10: Two furter visualisations of the Dalitz plot to make resonances better visual.

5.5 Local matter anti-matter differences

As we want to observe CP violation in charmless $B^\pm$ meson decays, we need to cut out both of the resonances, as they include charm quarks. This is done by applying a cut on the mass as

$$(m_{\text{Res}} > 1890\,\text{MeV}) \quad \text{or} \quad (m_{\text{Res}} < 1830\,\text{MeV})$$
$$\text{and}$$
$$(m_{\text{Res}} > 3440\,\text{MeV}) \quad \text{or} \quad (m_{\text{Res}} < 3390\,\text{MeV}).$$

The Dalitz plot after and before removing the most significant resonances is shown in Figure 11. No clear band structures are visible anymore. The CP asymmetry is evaluated for different kinematic regions now. To do this, the dataset is splitted for positively and negatively charged B mesons. The binned dalitz plots for each dataset are shown in Figure 12. The counts for each bin are extracted and used to calculate the CP asymmetry bin-wise. The CP asymmetry for each bin is shown in Figure 13. The resulting CP asymmetry can be misleading, if the statistic in the relative bin is too low. To prevent this and extract a meaningful conclusion, the uncertainty and significance per bin is calculated and shown in Figure 14. As can be seen in Figure 14 and Figure 13, the lower kinematic region shows high significance and asymmetry. This region is extracted by applying a cut as

$$(m_{\text{Low}} < 2000\,\text{MeV}) \quad \text{and} \quad (m_{\text{High}} > 2287\,\text{MeV}) \quad \text{and} \quad (m_{\text{High}} < 4067\,\text{MeV})$$

This corresponds to the first three bins in the x-axis and the third to ninth bin in the y-axis. The mass distribution of the B^+ and B^- mesons are shown in Figure 15. The
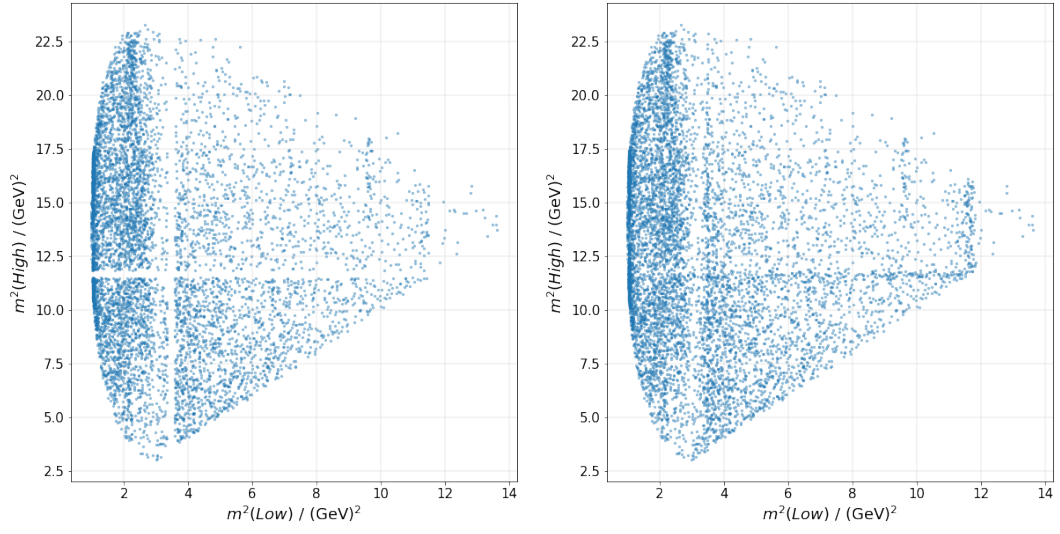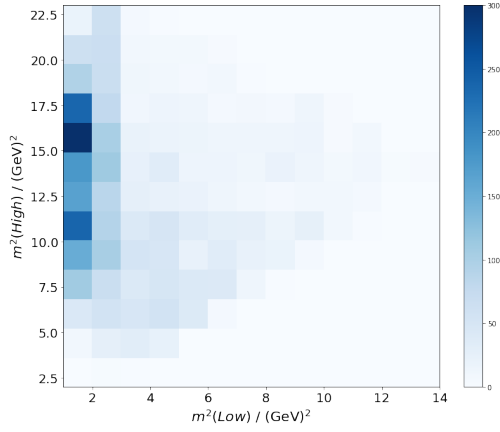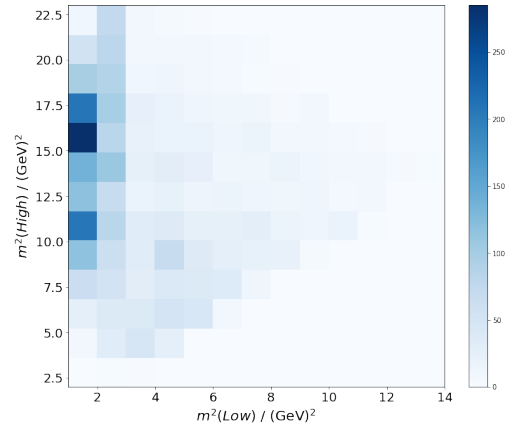
13

Figure 11: Dalitz plots after (left) and before (right) removing charm resonances.

(a) Binned Dalitz plot of the recorded data including only decays of B^+.

(b) Binned Dalitz plot to visualise local densities.

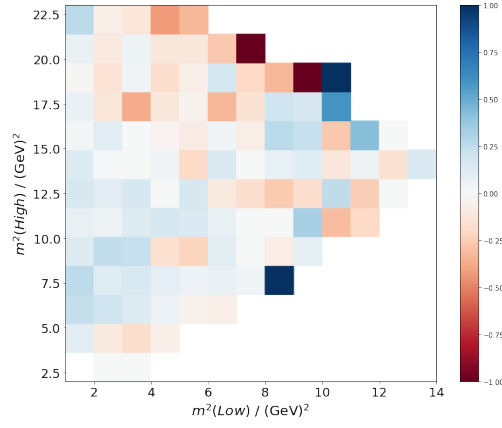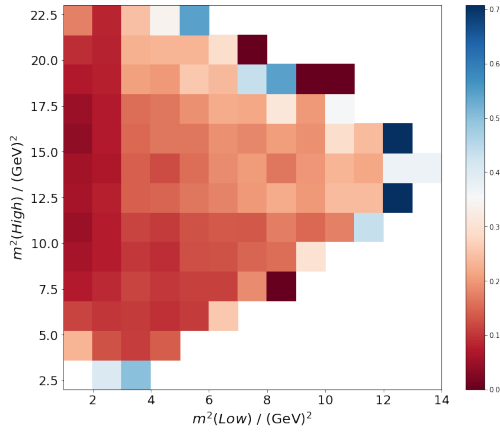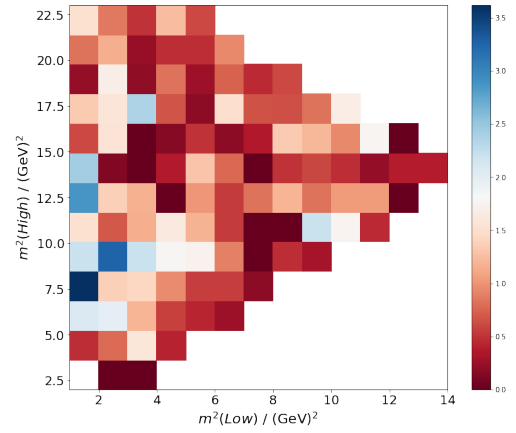**Figure 12:** Binned Dalitz plot of the recorded data including only decays of B^-.

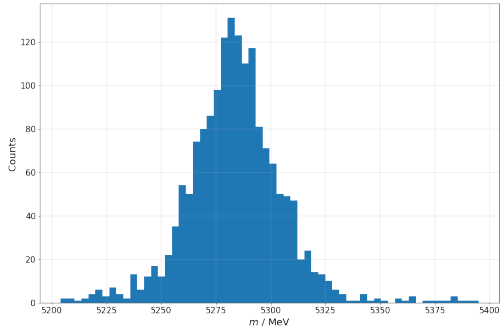**Figure 13:** Binned *CP* asymmetry for the recorded data.

(a) Binned uncertainty of the *CP* asymmetry for the recorded data.
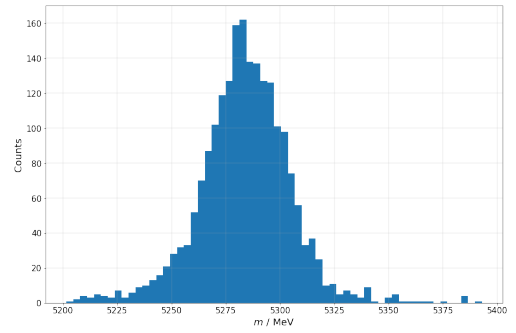

(b) Binned significance of the *CP* asymmetry for the recorded data.

Figure 14: Binned uncertainty and significance for the caluclated *CP* asymmetry.

(a) Invariant mass distribution for B^-.

(b) Invariant mass distribution for B^-.

Figure 15: Distributions of the invariant mass of the $B^\pm$ candidates in the relevant bins of the Dalitz plot.

15

resulting local *CP* asymmetry corrected by the production asymmetry, the uncertainty and the significance are

$$A_{CP,\text{loc}} = 0.1129$$

$$\sigma_{A_{CP,\text{loc}}} = 0.0195$$

$$S_{A_{CP,\text{loc}}} = 5.2748.$$

The found local *CP* asymmetry can therefore be called a discovery.

6 Discussion

In this analysis, the global *CP* asymmetry for the decays $B^{\pm} \to K^{\pm}K^+K^-$ is determined as $A_{CP,\text{global}} = 0.0336 \pm 0.0154$ with a significance of $S_{A_{CP,\text{global}}} = 2.181$. In the 2013 LHCb analysis on the same dataset, the global *CP* asymmetry is determined as $A_{CP}(B^{\pm} \to K^{\pm} K^+K^-) = -0.043 \pm 0.009 \text{ (sys)} \pm 0.003 \text{ (stat)} \pm 0.007(J\psi K^{\pm})$ with a significance of 3.7σ [1]. The opposite sign of the asymmetry is due to an opposite definition of the asymmetry observable in Equation 1. Considering the uncertainty of the *CP* asymmetry determined in this analysis, the values are in agreement with each other. Although systematic uncertainties apart from the estimated production asymmetry were neglected in this analysis and were, however, included in the LHCb analysis, the uncertainties of the LHCb value lie clearly under the uncertainty statet here. This can be explained by the fact, that the analysis here was strongly simplified and selection criteria were not optimised as much as in the LHCb paper. This also results in a lower significance. By viewing the Dalitz plots of the two-Kaon masses, resonances at approximately $1870 \,\text{MeV}$ and $3390 \,\text{MeV}$ are observed and can be identified with D^0 and χ_{c0} contributions. In the original paper, only the D^0 resonance is accounted for and removed. The strongest local *CP* asymmetry here is observed in low $m(KK)$ regions which is in agreement to the observations in Ref. [1]. The strongest local *CP* asymmetry follows as $A_{CP,\text{loc}} = 0.1129 \pm 0.0195$ with a significance of 5.2σ. In the LHCb analysis, the *CP* asymmetry in low $m(KK)$ regions reads $A_{CP}^{\text{reg}}(KKK) = -0.226 \pm 0.020 \text{ (sys)} \pm 0.004 \text{ (stat)} \pm 0.007(J\psi K^{\pm})$ [1]. Here, the values are not in agreement, considering the given uncertainties. However, the uncertainty of the value from this analysis is clearly underestimated since no systematic uncertainties are included apart from the estimated production asymmetry of $1\,\%$. Following from that, the claimed significance of 5.2σ is overestimated. Further, the differences in the observed values could originate from different binning or different mass criteria of the low mass regions as defined in the LHCb paper and here.

All in all, the results achieved in this simplified *CP* violation analysis are in good agreement with the LHCb observations on the same data. The neglection of systematic uncertainties and different selection criteria can explain the deviations of the observed asymmetries.

References

[1] R Aaij et al. 'Measurement of CP violation in the phase space of $B^\pm \to K^\pm \pi^+ \pi^-$ and $B^\pm \to K^\pm K^+ K^-$ decays'. In: *Phys. Rev. Lett.* 111 (2013), p. 101801. DOI: 10.1103/PhysRevLett.111.101801. arXiv: 1306.1246 [hep-ex].

[2] A. Augusto Alves Jr. et al. 'The LHCb Detector at the LHC'. In: *JINST* 3 (2008), S08005. DOI: 10.1088/1748-0221/3/08/S08005.

[3] Rene Brun and Fons Rademakers. *ROOT - An Object Oriented Data Analysis Framework.* 1997. URL: https://root.cern.ch/.

[4] Nicola Cabibbo. 'Unitary Symmetry and Leptonic Decays'. In: *Phys. Rev. Lett.* 10 (12 June 1963), pp. 531–533. DOI: 10.1103/PhysRevLett.10.531. URL: https://link.aps.org/doi/10.1103/PhysRevLett.10.531.

[5] J. H. Christenson et al. 'Evidence for the 2π Decay of the K_2^0 Meson'. In: *Phys. Rev. Lett.* 13 (4 July 1964), pp. 138–140. DOI: 10.1103/PhysRevLett.13.138. URL: https://link.aps.org/doi/10.1103/PhysRevLett.13.138.

[6] S. L. Glashow, J. Iliopoulos and L. Maiani. 'Weak Interactions with Lepton-Hadron Symmetry'. In: *Phys. Rev. D* 2 (7 Oct. 1970), pp. 1285–1292. DOI: 10.1103/PhysRevD.2.1285. URL: https://link.aps.org/doi/10.1103/PhysRevD.2.1285.

[7] Makoto Kobayashi and Toshihide Maskawa. 'CP-Violation in the Renormalizable Theory of Weak Interaction'. In: *Progress of Theoretical Physics* 49.2 (Feb. 1973), pp. 652–657. ISSN: 0033-068X. DOI: 10.1143/PTP.49.652. eprint: https://academic.oup.com/ptp/article-pdf/49/2/652/5257692/49-2-652.pdf. URL: https://doi.org/10.1143/PTP.49.652.

[8] *Measurement of matter-antimatter asymmetries with the LHCb experiment.* TU Dortmund, Faculty of Physics, AG Albrecht. 2022. URL: https://moodle.tu-dortmund.de/pluginfile.php/2306063/mod_resource/content/1/LHCb-CPV.pdf.

[9] A. D. Sakharov. 'Violation of CP Invariance, C asymmetry, and baryon asymmetry of the universe'. In: *Pisma Zh. Eksp. Teor. Fiz.* 5 (1967), pp. 32–35. DOI: 10.1070/PU1991v034n05ABEH002497.

[10] *The Review of Particle Physics (2024).* Particle Data Group. URL: https://pdglive.lbl.gov/Viewer.action (visited on 12/06/2024).